Journal of Structural Geology 32 (2010) 1170–1184

Contents lists available at ScienceDirect

Journal of Structural Geology

journal homepage: www.elsevier.com/locate/jsg

Kinematic analysis of asymmetric folds in competent layers using mathematical modelling☆

J. Aller [a,*], N.C. Bobillo-Ares [b], F. Bastida [a], R.J. Lisle [c], C.O. Menéndez [b]

[a] Departamento de Geología, Universidad de Oviedo, Jesús Arias de Velasco s/n, 33005 Oviedo, Spain
[b] Departamento de Matemáticas, Universidad de Oviedo, 33007 Oviedo, Spain
[c] School of Earth and Ocean Sciences, Cardiff University, Cardiff CF10 3YE, UK

ARTICLE INFO

Article history:
Received 18 December 2009
Received in revised form
28 June 2010
Accepted 27 July 2010
Available online 5 August 2010

Keywords:
Folding
Strain
Mathematical modelling
Recumbent folds

ABSTRACT

Mathematical 2D modelling of asymmetric folds is carried out by applying a combination of different kinematic folding mechanisms: tangential longitudinal strain, flexural flow and homogeneous deformation. The main source of fold asymmetry is discovered to be due to the superimposition of a general homogeneous deformation on buckle folds that typically produces a migration of the hinge point. Forward modelling is performed mathematically using the software 'FoldModeler', by the superimposition of simple shear or a combination of simple shear and irrotational strain on initial buckle folds. The resulting folds are Ramsay class 1C folds, comparable to those formed by symmetric flattening, but with different length of limbs and layer thickness asymmetry. Inverse modelling is made by fitting the natural fold to a computer-simulated fold. A problem of this modelling is the search for the most appropriate homogeneous deformation to be superimposed on the initial fold. A comparative analysis of the irrotational and rotational deformations is made in order to find the deformation which best simulates the shapes and attitudes of natural folds.

Modelling of recumbent folds suggests that optimal conditions for their development are: a) buckling in a simple shear regime with a sub-horizontal shear direction and layering gently dipping towards this direction; b) kinematic amplification due to superimposition of a combination of simple shear and irrotational strain with a sub-vertical maximum shortening direction for the latter component. The modelling shows that the amount of homogeneous strain necessary for the development of recumbent folds is much less when an irrotational strain component is superimposed at this stage that when the superimposed strain is only simple shear. In nature, the amount of the irrotational strain component probably increases during the development of the fold as a consequence of the increasing influence of the gravity due to the tectonic superimposition of rocks.

1. Introduction

Kinematic studies of folding are concerned with different types of strain patterns that appear in folded layers and the geometrical evolution of the folded layers from the initial, undeformed stage to the final fold. Kinematic folding mechanisms can be considered to be the theoretical tools that can be used in this analysis; they define rules that determine the displacements to be produced and the final strain pattern inside the folded layers. A reasonable starting point for establishing basic folding mechanisms is the experimental production of folds, comparable to natural ones. For example, the classical folding experiments by Kuenen and de Sitter (1938) using sheets of paper and rubber revealed the operation of the mechanisms that we now refer to as the flexural and tangential longitudinal strain mechanisms respectively. From this type of experiments it is possible to define the kinematic mechanisms as theoretical idealizations that can be mathematically analysed. In this way, applying the conditions required by every mechanism it is possible, from an initial configuration of a layer, to model theoretically the geometry of a folded layer and its strain pattern. The folding necessarily involves heterogeneous deformation; however, the superimposition of a homogeneous strain during folding can significantly modify the geometry of folds and their strain pattern, and this type of modification can be included as a folding mechanism in its own right.

An interesting aspect of folding kinematics is concerned with the development of asymmetric folds. According to the definition

☆ The program code ("FoldModeler") can be found in the following web page: http://www.geol.uniovi.es/Investigacion/OFAG/Foldteam.html

* Corresponding author. Fax: +34 98 510 3103.
E-mail address: aller@geol.uniovi.es (J. Aller).

0191-8141/$ – see front matter © 2010 Elsevier Ltd. All rights reserved.
doi:10.1016/j.jsg.2010.07.008

given by most authors, a fold is asymmetric when it lacks bilateral symmetry about the axial plane (Turner and Weiss, 1963, p. 122; De Sitter, 1964, p.272; Whitten, 1966, p. 601; Ramsay, 1967, p. 351). Most of the folds found in rocks are asymmetric and in many cases the degree of asymmetry is very high. Good examples are the major recumbent folds common in the hinterland of orogenic belts, the folds developed in ductile shear zones, and parasitic folds developed on the limbs of major folds. These examples illustrate the importance of gaining understanding of the folding mechanisms operating during the formation of asymmetric folds in order to further our knowledge of orogenic deformation. Most of the available studies on natural asymmetric folds place special emphasis on the shape and asymmetry of the folded surfaces or layers, but the final strain patterns or the characteristics of the progressive deformation in these folds are poorly known.

The aim of this paper is to study some general aspects of the kinematics of asymmetric folds in competent layers. Theoretical folds are modelled using tangential longitudinal strain, flexural flow and homogeneous strain. The asymmetry can be introduced via all three mechanisms. Superimposition on pre-existing folds of a general homogeneous strain, with final principal directions freely chosen will be the main source of asymmetry in our models. This modelling yields information about the final strain distributions and the progressive deformation in asymmetric folds (forward problem), and the potential for ascertaining the kinematic mechanisms that operated in specific natural asymmetric folds (inverse problem), by comparison of the geometry of these folds with theoretically modelled folds. A special attention is devoted to large recumbent folds, because they are key pieces for understanding of the structure of orogens.

The analysis is two-dimensional, considering strain in the profile plane of the folded layer. Application of the theoretically modelled folds to the analysis of the mechanisms that operate in natural folds is limited by the availability of strain measurements in the rocks. Fortunately, detailed information on the natural fold geometry and the cleavage pattern provides very useful data that can be related to the strain state and the kinematic mechanisms involved in the development of asymmetric folds.

2. On the description of asymmetric folds

A qualitative description of fold asymmetry was made by Ramsay (1967, pp. 351–352) using the letters M (symmetric), S or Z (asymmetric), in such a way that the shape of the letter describes the shape of the fold. This method is useful for the mapping of major structures from parasitic folds. From a quantitative point of view, Loudon (1964) and Whitten (1966) proposed the use of the third statistical moment of the orientation distribution of the normals to the folded surface profile to express the asymmetry of folds. Since the asymmetry depends on the relative length of the fold limbs (Ramsay, 1967, p. 351), a simple measure of the asymmetry of a fold is the ratio between these lengths. Tripathi and Gairola (1999) define the degree of asymmetry of a folded surface as the sum of two parameters, one depending on the difference in amplitude and other depending on the difference in shape. A problem with this method is that this parameter does not express the extent to which the asymmetry is due to differences in shape or differences in amplitude. In order to represent graphically the fold asymmetry in a 2D coordinate system, it is necessary to describe this geometrical feature using only two parameters. A complete description of the asymmetry of folded surfaces is not really possible with only two parameters; in fact, Twiss (1988) proposed a classification which requires six parameters for profiles of general asymmetric folded surfaces. Nevertheless, the most relevant features of this asymmetry can be characterised by the following parameters (Bastida et al., 2005; Lisle et al., 2006):

$$\text{Shape asymmetry}: S_a = A_F/A_B \tag{1}$$

$$\text{Amplitude asymmetry}: A_a = y_{0F}/y_{0B} \tag{2}$$

where A_F and A_B are the respective normalized areas (Bastida et al., 1999) of the forelimb and the backlimb (defined as the steeper and gentler limb respectively), and y_{0F} and y_{0B} are the y_0 parameters of the forelimb and the backlimb, respectively (Fig. 1a). The plot of these parameters in a graph of S_a against A_a for all the folds of a specific set, allows the visualization of the variation in asymmetry of these folds.

In order to analyse the asymmetry of the folded layer, comparison of the curves representative of the two limbs in the classifications of Ramsay (1967, pp. 359–372), Hudleston (1973) or Treagus (1982) can give a qualitative idea of the shape asymmetry. A simple parameter to quantify this aspect of asymmetry is the thickness asymmetry (T_a) (Fig. 1b), defined as the ratio between the orthogonal thickness of the forelimb and that of the backlimb for the maximum dip in the Ramsay's classification.

3. Modelling asymmetric folds: preliminary considerations

For the theoretical study of folding kinematics in individual competent layers it is opportune to use an auxiliary reference line, termed the 'guideline', which is usually, but not necessarily, positioned midway between the layer boundaries in the initial configuration. The guideline facilitates the monitoring of the layer geometry during folding. To analyse the strain in a folded layer profile it is necessary to choose a function to describe the form of the guideline. In this paper we will use functions of the conic section family (Aller et al., 2004). The conic sections have important advantages over other families of functions. They offer a good fit to the most common fold shapes and have finite curvature at all of their

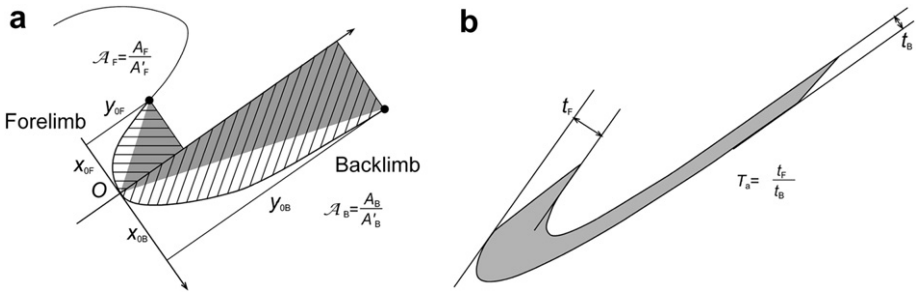

Fig. 1. (a) Parameters to characterise asymmetry in folded surfaces. The normalized area A for a fold limb is the ratio between the area A (lined) defined by the limb and the area A' (gray) of the chevron fold with the same x_0 and y_0 parameters. (b) Thickness ratio (T_a) as a measure of asymmetry in folded layers.

points, a continuous change of curvature, a curvature extreme value in the apex, and at least one axis of symmetry. An important additional advantage of the conics is that affine transformations (homogeneous deformation) map ellipses to ellipses, parabolas to parabolas and hyperbolas to hyperbolas (Brannan et al., 1999, p. 85). This characteristic property of the conics makes it possible to analyse cases in which a general homogeneous strain operates during the development of asymmetric folds and modifies the geometry of the folded surface profile. In these cases, if the curves that describe the folded guideline before and after strain belong to different families, the change in shape is very difficult to describe, and a thorny problem arises in the analysis of the folding kinematics. The conics are simple curves that do not pose this problem, and this makes them our preferred choice.

In the case of symmetric folds it is only necessary to analyse a single limb for each fold, so that the guideline is defined by a sector of a conic in an interval [0, x_0], where x_0 is the limb width (Bobillo-Ares et al., 2004). However, for the theoretical modelling of asymmetric folds, both limbs need to be considered. In this case, the two limbs need to be modelled together by a single conic section, since the hinge point can migrate along the guideline, and consequently a material point can migrate from one limb to the other during the development of the fold. The coordinate origin is located at the vertex (hinge point) of the conic section and the folds are modelled as synforms with the coordinate axes as shown in Fig. 1a. This x-axis is considered as horizontal reference datum for the measurement of line inclinations and layer dips in the analysis. The considered part of the conic is characterised by the eccentricity, a scale factor, and the interval over which it is defined. Alternatively it can be useful to use, instead of the scale factor, a normalized amplitude (or aspect ratio) h of the right limb, defined as the ratio between the height and the width of this limb (y_{0B}/x_{0B}; see Fig. 1a).

One result of the kinematic analysis of asymmetric folds is to obtain the strain distribution in the folded layer. For the application of this analysis to natural folds, we assume that the major axis of the strain ellipse has the direction of the cleavage trace on the fold profile, as commonly suggested, at least as an approximation (e.g., Siddans, 1972; Wood, 1974; Passchier and Trouw, 2005, p. 94). In agreement with the available data (e.g., Southwick, 1987; Passchier and Trouw, 2005, p. 95), we assume that cleavage development requires a minimum shortening normal to the cleavage of 30% ($R = \sqrt{\lambda_1/\lambda_2} \approx 2$ for isochoric deformation). The presence of cleavage is necessary for an adequate kinematic interpretation of natural asymmetric folds.

4. Kinematic mechanisms producing asymmetric folds: mathematical modelling

Considering individual competent layers and assuming folding as a result of a single progressive deformation episode, we can distinguish two sources of asymmetry in folds: a) asymmetry induced during the active folding, and b) asymmetry induced by superimposition of homogeneous deformation on pre-existing folds.

4.1. Asymmetry induced during the active folding

Two main mechanisms can be considered during this folding stage.

4.1.1. Tangential longitudinal strain (TLS) (or neutral surface folding)

This mechanism was introduced early in structural geology (e.g., Ickes, 1923). It is the mechanism assumed in the basic buckling theory of competent members (elastic or viscous) (e.g., Ramberg, 1960; Biot, 1961; Currie et al., 1962). Two modes of this mechanism have been considered: equiareal tangential longitudinal strain (ETLS) and parallel tangential longitudinal strain (PTLS), which involves area change. The former has been defined by Ramsay (1967, p. 397) and it involves no area change; it does not conserve exactly the orthogonal thickness of the folded layers (Bobillo-Ares et al., 2000). The latter is usually assumed in buckling theory and it has been considered in the analysis of natural folds by several authors (Hudleston and Holst, 1984; Hudleston and Tabor, 1988; Hudleston and Srivastava, 1997; Ormand and Hudleston, 2003; Bobillo-Ares et al., 2006; Lisle et al., 2009); it produces perfect parallel folds.

4.1.2. Flexural flow (FF)

The term “flexural flow” was introduced in structural geology by Donath (1963) and Donath and Parker (1964) to define a folding mechanism that involves a flow within individual layers giving rise to a thickening of the hinge zone with respect to the limbs. Subsequently, Ramsay (1967, p. 392) redefined this mechanism as due to a continuous heterogeneous simple shear parallel to the boundaries of the layer so that the shear is null at the hinge points and increases in absolute value as the dip of the limb increases; it gives rise to parallel folds in which the area on the fold profile and the arc length of the boundaries or the fibres parallel to them are conserved. This is the sense given here to this mechanism. The deformation involved in FF is well known in strength of materials and it was described as the deflection of a beam or plate produced by shearing stresses parallel to their boundaries (e.g., Timoshenko, 1940, pp. 170–174). Some kinematic or mechanical models have been proposed to produce folds, mainly chevron folds, by FF (Smythe, 1971; Ramsay, 1974). Nevertheless, some authors (Price and Cosgrove, 1990, p. 250; Weijermars, 1992; Hudleston et al., 1996) have suggested that this mechanism requires a high mechanical anisotropy and Hudleston et al. (1996) have discussed, using finite-element models, the viability of FF in nature. They concluded that it is unlikely that competent layers would be sufficiently anisotropic as to develop a significant component of flexural fold during folding. Toimil and Fernández (2007), analysing by computer the kinematics of symmetric natural folds in competent layers, conclude that FF is much less important than TLS and it can occur after the latter as a small component due to geometrical incompatibilities generated during TLS. Bastida et al. (2007) mathematically modelled the kinematics of chevron folds and concluded that, in general, FF is necessary at the last stage of buckling, although the increment of folding due to this mechanism can be very small. In contrast with the subsidiary character of the FF suggested in these papers, Ormand and Hudleston (2003), analysing the meso and microstructures in two folds developed in single competent layers of limestone, inferred that they were formed by asymmetric FF. Given this background, although FF could be a subordinate contributor, it is used to model asymmetric folds in this study.

Asymmetry produced in folds during the initiation and development of active folding has been analysed from a mechanic point of view by several authors (Ghosh, 1966; Price, 1967; Treagus, 1973; Anthony and Wickham, 1978; Manz and Wickham, 1978; Frehner and Schmalholz, 2006; Treagus and Fletcher, 2009) and it has been attributed to the action of a principal compressive stress oblique to the competent layer. On the other hand, experimental or finite-element results show that the asymmetry of the folds is small or even null (Ghosh, 1966; Anthony and Wickham, 1978; Manz and Wickham, 1978).

Modelling of equiareal and parallel TLS mechanisms is performed in this paper using the geometrical transformations developed by Bobillo-Ares et al. (2000, 2006) and modelling of FF

mechanism is carried out in the same manner as in Bastida et al. (2003). The asymmetry induced for these mechanisms can be simulated theoretically by positioning the hinge points of the folded layer boundaries so that they do not coincide with points that are equidistant from the ends of the layer. Asymmetries in the strain distribution due to flexural flow with the pin line on a limb of the fold have been proposed by several authors (Geiser et al., 1988; Fisher and Anastasio, 1994; Ormand and Hudleston, 2003), but have not been considered in the present study.

4.2. Asymmetry induced by superimposition of homogeneous deformation on pre-existing folds

Following the pioneering analyses of flattened folds (Ramsay, 1962, 1967, pp. 411–415; De Sitter, 1964, pp. 274–277; Mukhopadhyay, 1965), homogeneous strain superimposed on pre-existing folds has been widely considered to be a common mechanism for explaining Ramsay class 1C folds. In general, this flattening strain will bring about an asymmetry in a pre-existent fold when the axes of superimposed strain ellipse are oblique to the axial plane. Two categories of superimposed oblique homogeneous strain with different geological significance can be distinguished:

Irrotational deformation (sensu Ramsay, 1967, pp.60–61). This was described by Hudleston (1973) as oblique flattening. The strain involved can be pure shear or irrotational strain with area change. It is defined by the angle between the major axis of the strain ellipse and the axial surface trace of the pre-existing fold and the principal strain values λ_1 and λ_2 (or one of them and the area change value).

Rotational deformation (sensu Ramsay, 1967, pp.60–61). This is defined by the four components of the corresponding deformation gradient. Among the infinite number of possible superimposed strains, the following have been considered of special geological relevance:

- *Simple shear*. This has been considered as a suitable folding mechanism in several geological situations (Hudleston, 1977; Sanderson, 1979; Cobbold and Quinquis, 1980; Ramsay, 1980; Ramsay et al., 1983; Ramsay and Huber, 1987, pp. 597–598; Srivastava and Srivastava, 1988; Casey and Dietrich, 1997; Ez, 2000; Harris et al., 2002; Carreras et al., 2005; Alsop and Carreras, 2007). This type of homogeneous deformation has the advantage of accommodating a continuous strain gradient across the shear plane.
- *Combination of homogeneous simple shear and irrotational deformation*. This has been considered by many authors as a deformation history common in several geological situations in which folds can be kinematically amplified (Ramberg, 1975; Ramsay, 1980; Sanderson, 1982; De Paor, 1983; Ridley and Casey, 1989; Fossen and Tikoff, 1993; Simpson and De Paor, 1993; Tikoff and Fossen, 1993, 1996; Carreras et al., 2005).

The irrotational component can have its direction of maximum stretch parallel or perpendicular to the shear direction of the simple shear and it can involve area change or no area change (pure shear) on the fold profile. Taking into account that the application order of the deformations has an influence on the final result, there are three main possibilities: simple shear followed by irrotational strain, irrotational strain followed by simple shear and simultaneous simple shear and irrotational strain. Some authors have discussed the simultaneous case (Fossen and Tikoff, 1993; Tikoff and Fossen, 1993; Merle, 1994). From the study of Ramberg (1975), and for a reference system with the x-axis in the shear direction of the simple shear component, these authors have obtained the following matrix for the material deformation gradient:

$$G = \begin{pmatrix} k_1 & \gamma\frac{k_1-k_2}{\ln(k_1/k_2)} \\ 0 & k_2 \end{pmatrix}. \quad (3)$$

The elements of the leading diagonal describe the components of irrotational strain and the off-diagonal non zero element describes the rotational component of the deformation. When $k_1 = k_2 = 1$, this element is not defined, but when k_1 is very slightly different than k_2 and than 1, the deformation is a simple shear; $\gamma = 0$ implies pure shear. A simple *ad hoc* derivation of matrix (3) is given in Appendix A. For the mathematical modelling of this mechanism, coordinates of points of the buckled layer must be left-hand multiplied by the matrix (3) to obtain the coordinates of points of the layer configuration after the superimposition of the homogeneous deformation.

The superimposition of a general homogeneous deformation on pre-existing folds can involve a migration of the hinge point along the guideline. Therefore, in order to obtain the equation of the conic that describes the new guideline it is necessary to make a coordinate transformation to take the coordinate origin to the new hinge point. This transformation is not a trivial task and it has been included in Appendix B.

By analysing the results of the superimposition of deformations given by different forms of the matrix (3) on the same pre-existing fold we can see that it is possible to obtain folds with the same shape but different attitudes, i.e., folds that only can be distinguished by a different value of the rotation of the principal strain direction.

5. Computer methods for modelling asymmetric folds

A new version of the 'FoldModeler' program (first presented by Bobillo-Ares et al., 2004) is used in this study to model asymmetric folds. This program is written in the MATHEMATICA™ environment, and it permits the modelling of folds involving the mechanisms considered above: TLS (ETLS and PTLS), FF and homogeneous deformation (Bobillo-Ares et al., 2004). These mechanisms can be superimposed in any order to produce a fold in the manner described by Bastida et al. (2003) and Bobillo-Ares et al. (2004) for symmetric folds. The main difference is that in the case of asymmetric folds the homogeneous deformation has a general character, so that it can be rotational or irrotational and its principal directions can have any orientation with respect to the geometrical elements of the pre-existent fold.

Theoretical modelling of a combination of kinematic mechanisms is made by a sequence of successive folding steps. The first stage in the computer modelling is to define the initial configuration of the layer profile to be folded. To make it, the profile is divided in a net of parallelograms so small as to allow the assumption of homogeneous strain within them. The net nodes define the points to be transformed by the different folding mechanisms, allowing the analysis of the strain in the folded layer.

Once the initial layer is defined, it is deformed by applying a number of folding steps. Every step corresponds to a specific mechanism and involves the application of the appropriate transformation relations to the nodes. Therefore, definition of a folding step requires specification of the folding mechanism involved and the changes that the step must produce in the guideline parameters (aspect ratio and shape variations).

Computer modelling of a general homogeneous deformation superimposed on folds involves the introduction of folding steps with the matrix of the corresponding material deformation gradient, whose four elements must be specified. In order to simplify this task and to ease interpretation, it is convenient to form

this matrix by a superimposition of others for simple deformations, such as the following:

- *Simple shear*. This can be imposed with any amount and in any direction. Its introduction requires specification of the value of the shear strain γ, and the shear direction.
- *Irrotational strain*. This is a general irrotational strain that can be applied with any amount and area change, and with principal directions freely selected. To apply this strain type, specification of the maximum principal stretch, $\sqrt{\lambda_1}$, the corresponding principal direction and the area change (final area/initial area) is required.
- *Area change*. This can be included as an independent element introducing a scale factor that multiplies the previous area.
- *Rigid body rotation*. This can be included as an independent element by specifying the rotation angle.

The above method produces deformations of very general character by superimposition of simple elements. On the other hand, by superposing very small increments it is also possible to model the simultaneity of two or more types of homogeneous deformation.

As a result of the superimposition of a finite number of steps, folds formed by a combination of several folding mechanisms are simulated. Among the information that FoldModeler provides we can mention the following:

1. A visual display of the folded layer, showing the net of deformed quadrilaterals, the distribution of the strain ellipses and their axes, and a variation in the gray level depending on the *R*-value ($R = \sqrt{\lambda_1/\lambda_2}$) of the strain ellipse.
2. θ–α graph. Curves showing the variation of the long axis inclination (θ) of the strain ellipse (measured anticlockwise from the positive *x*-axis between 0 and 180°) as a function of the layer dip (α) for the inner and outer arc of the folded layer.
3. R–α graph. Curves showing the variation of R as a function of the layer dip (α) for the inner and outer arc of the folded layer.
4. Ramsay's classification of the folded layer and the curve of the squared orthogonal thickness t'^2_α versus $\sin^2\alpha$.
5. Parameters s_1 and s_2 derived from the curve t'^2_α versus $\sin^2\alpha$ (Bastida et al., 2005).
6. The bulk shortening associated with folding.
7. The eccentricity of the final conic section of the guideline and the aspect ratio of each of the two limbs.
8. A graph describing the guideline curvature variation through the folded layer.
9. The ratio between the layer thickness at the hinge point (t_0) and the amplitude of the outer arc (y_{oa}).

6. Forward modelling of asymmetric folds

Combining the kinematic mechanisms included in the 'FoldModeler' program, we can model countless folds with different strain distributions. However, in this chapter we have chosen a few examples that we consider relevant from a geological point of view. Firstly, we consider briefly the modelling of asymmetric folds by the basic mechanisms of TLS (ETLS and PTLS) and FF. Later, we consider some superimposition models of a homogeneous strain on folds formed by TLS and/or FF.

6.1. Flexural-flow and tangential longitudinal strain

Unlike the modelling of these mechanisms in symmetric folds, in the case of asymmetric folds the two parts of the conic section representing the limbs will in general have different lengths and amplitudes and they will be determined for intervals of different length on the *x*-axis. In the computer modelling, these intervals are defined by specifying the number of quadrilaterals that must appear at each side of the hinge point in the initial configuration. Examples of asymmetric folds formed by FF and ETLS are shown in Fig. 2. In folds modelled by flexural flow, the pin line lies along the axial trace of the fold.

6.2. Superimposed homogeneous deformation

Among the infinite possibilities to make this superimposition, we have chosen two types of rotational homogeneous deformation that, as stated above, are geologically relevant. Nevertheless, we will analyse below the factorization of any finite rotational

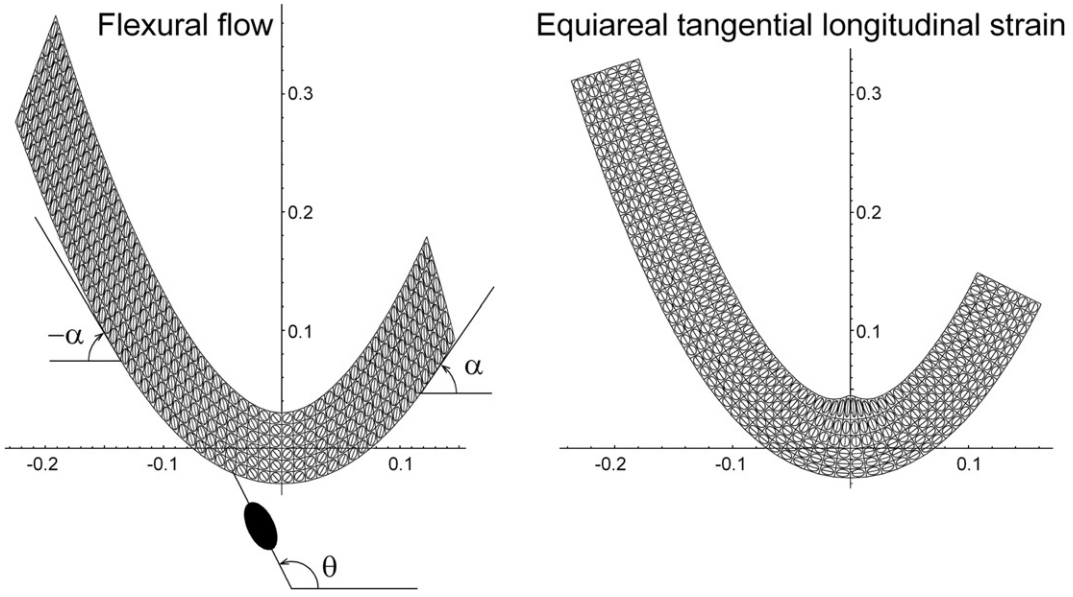

Fig. 2. Examples of asymmetric folds obtained with 'FoldModeler' and formed by flexural flow and equiareal tangential longitudinal strain with a parabolic guideline and aspect ratio for the right limb $h = 1$. Note the bulge in the inner arc of the hinge zone of the equiareal tangential longitudinal strain fold.

deformation in an irrotational strain followed by a rotation. This analysis allows obtaining the irrotational strain that can produce a fold with the same strain pattern originated by a specific rotational deformation.

6.2.1. Folds formed by superimposition of homogeneous simple shear on buckle folds

The geometry of folds formed by superimposition of homogeneous simple shear on folds formed by layer parallel shortening, flexural flow and/or tangential longitudinal strain mainly depends on the orientation of the shear direction with respect to the axial surface, the shear strain value γ (or the R-value of the superimposed strain ellipse) and the amplitude of the pre-existing fold. Two examples of the progressive development of these folds can be seen in Figs. 3 and 4. An essential feature of the folds obtained is that the migration of the hinge zone of the buckle fold towards one of the limbs during the shearing produces some characteristic features on this limb: a) a minimum of strain ratio, R, in flexural flow folds and in the outer arc of tangential longitudinal strain folds and a maximum of R in the inner arc of tangential longitudinal strain folds; b) as shown by the $\theta-\alpha$ curves, there exists a characteristic tendency to develop a parallelism between the major axis of strain ellipse and the axial plane with increasing γ, but the limb towards which the hinge migrates shows a resistance to develop this pattern in flexural folds and in the outer arc of tangential longitudinal strain folds, whereas the pattern is readily formed in the inner arc of tangential longitudinal strain folds.

The folds developed by superimposition of homogeneous simple shear on parallel or sub-parallel folds are class 1C, and they can be distinguished from parallel folds flattened by an irrotational strain with maximum shortening direction perpendicular to the axial surface, by the different length of the $t'_\alpha - \alpha$ curves of the Ramsay's classification of the two limbs or by the thickness asymmetry (T_a). For identical starting folds, another difference is the final attitude of the folds. Comparison of folds developed by superimposition of homogeneous simple shear on parallel folds with those developed by oblique flattening of parallel folds is complex and it is analysed below in the inverse modelling section. Assuming a horizontal shear direction, limbs of the pre-existing folds dipping opposite to the shear direction (considered on the top of the deformed body) will undergo a progressive thinning as the shear strain γ increases, and limbs of the previous folds dipping in the shear direction will first undergo thickening and later, if γ reaches a sufficiently high value, the layer acquires a dip opposite to the shear direction and progressive thinning occurs.

The fold prior to the superimposition of the homogeneous strain can be formed by a combination of layer parallel shortening, FF and/or TLS. For high γ values, it can be difficult to distinguish the folds produced by FF or TLS mechanisms acting in early stages of folding, but if the γ value is not high, the initial operation of the FF or TLS can be distinguished. Among other differences, FF gives rise to folds with the same $\theta-\alpha$ and $R-\alpha$ curves for the inner and outer arcs, whereas TLS produces different curves for both arcs (Figs. 3 and 4).

6.2.2. Folds formed by a combination of simultaneous homogeneous simple shear and irrotational strain on buckle folds

In this case, many possible combinations of the two components of the homogeneous deformation are possible. A model with the direction of maximum stretch of the irrotational component coinciding with the shear direction of the simple shear component

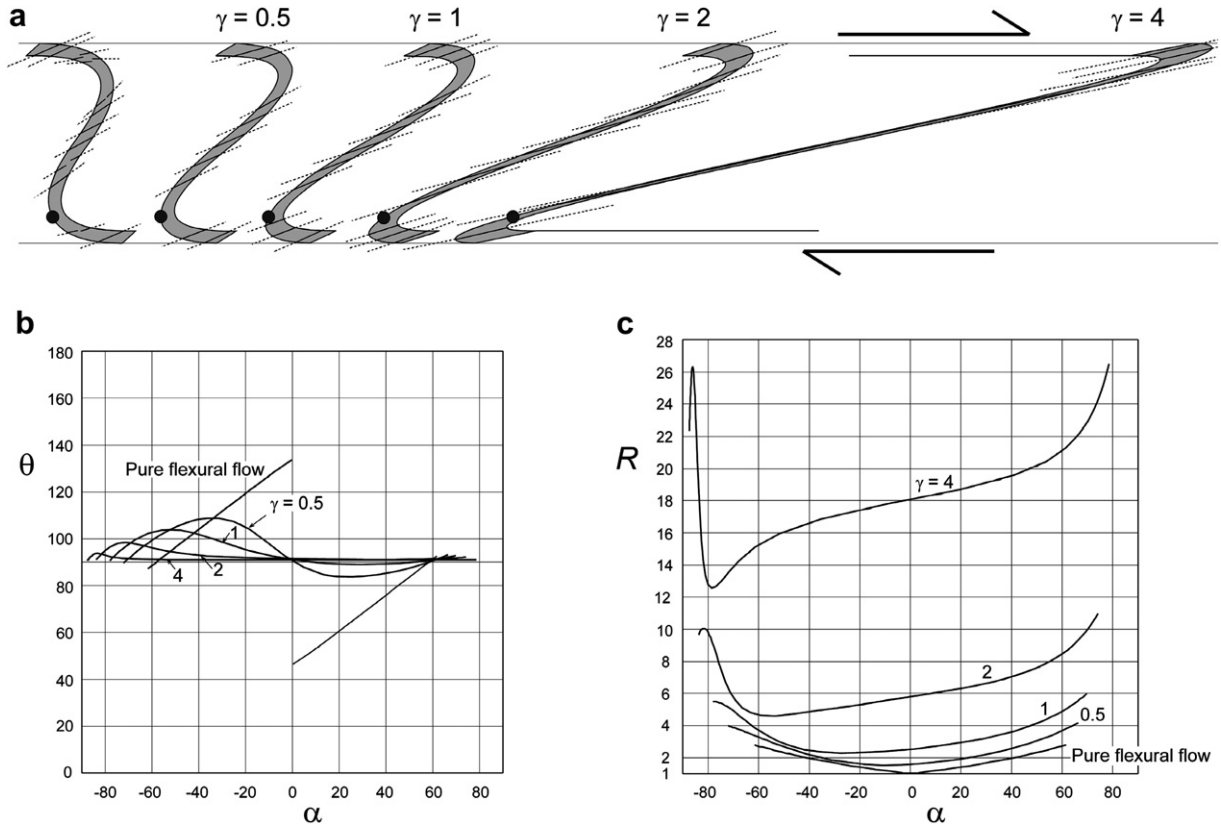

Fig. 3. a) Folds obtained with 'FoldModeler' for superimposed simple shear on flexural flow folds with a parabolic guideline and aspect ratio $h = 1$. Lines intersecting the fold profile are trajectories of the maximum finite elongation obtained for the numerical folds. Dark circles show the migration of the hinge zone of the initial fold along the forelimb with progressive shearing. b) $\theta-\alpha$ curves for the initial and the sheared folds. c) $R-\alpha$ curves for the initial and the sheared folds.

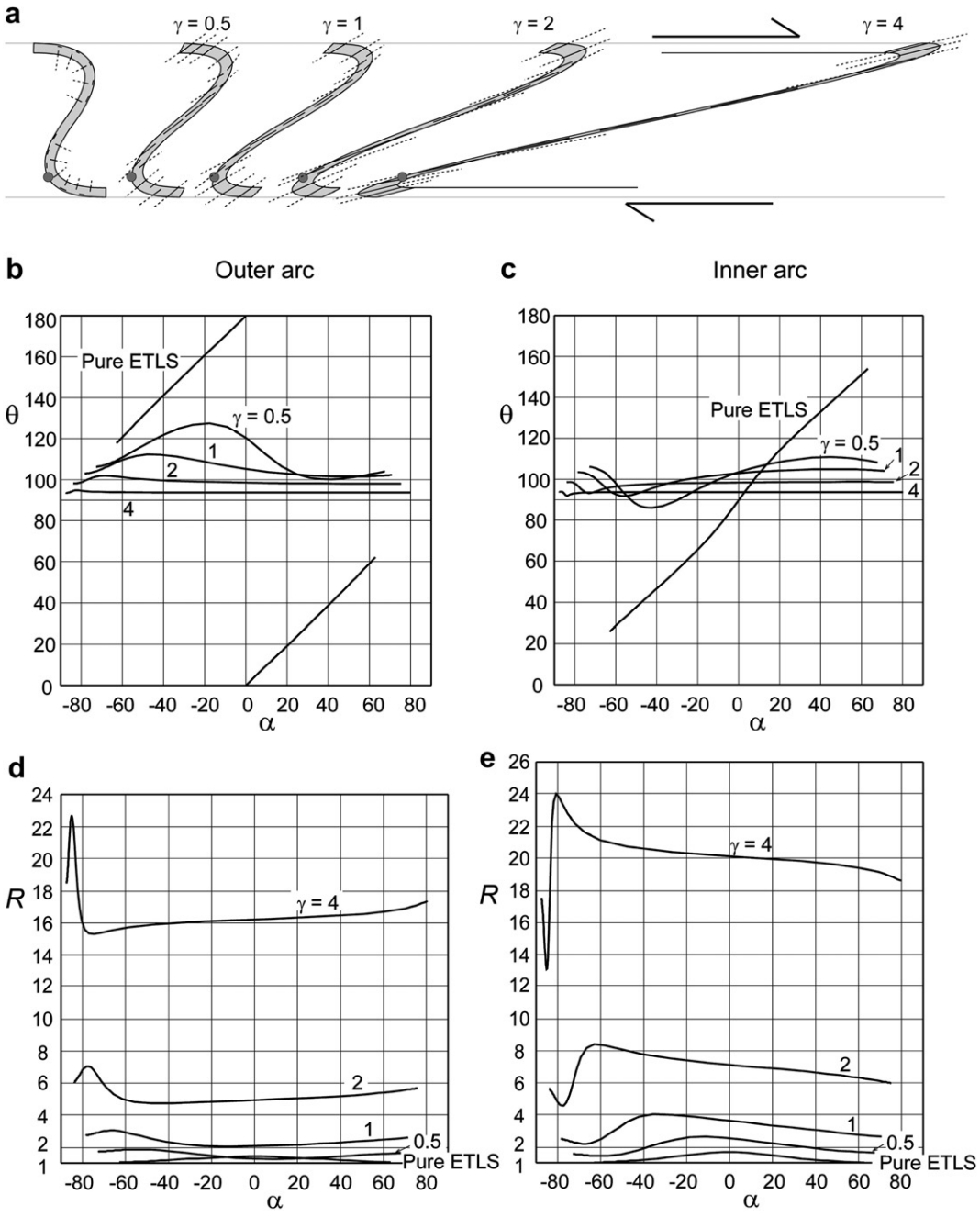

Fig. 4. a) Equiareal tangential longitudinal strain folds with a superimposed simple shear modelled with 'FoldModeler'. The initial buckling folds have a parabolic guideline and aspect ratio $h = 1$. Lines intersecting the fold profile are trajectories of the maximum finite elongation obtained for the numerical folds. Dark circles show the migration of the hinge zone of the initial fold along the forelimb with progressive shearing. b) and c) $\theta-\alpha$ curves for the outer and the inner arc of the initial and the sheared folds. d) and e) $R-\alpha$ curves for the outer and the inner arc of the initial and the sheared folds.

is shown in Fig. 5. As a general tendency, for the same final superimposed strain, folds formed by a superimposition on buckle folds of a combination of horizontal simple shear and irrotational strain with horizontal direction of maximum stretch have a gentler dipping axial plane and a thicker forelimb than folds formed by a superimposition of horizontal simple shear on buckle folds. Another model with the direction of maximum stretch of the irrotational component perpendicular to the shear direction of the simple shear component is shown in Fig. 6. In general, folds formed in this way have a steeper axial plane and a more symmetric character than folds formed by a superimposition of horizontal simple shear on buckle folds.

7. Inverse modelling of asymmetric folds

The aim of the inverse modelling is to determine the kinematic mechanisms that operated in a specific asymmetric fold. It requires fitting this fold, and the corresponding $\phi-\alpha$ and $R-\alpha$ curves, to a fold simulated using 'FoldModeler'. To make this task, it is necessary to collect all relevant information about the natural fold, as geometry of the folded surfaces and layers, the pattern of cleavage distribution, vorticity gauges, strain measures if possible and observations on structures related to folding mechanisms (wedge-like gashes opening towards the outer arc in the hinge zone, a cleavage better developed near the inner arc of the hinge

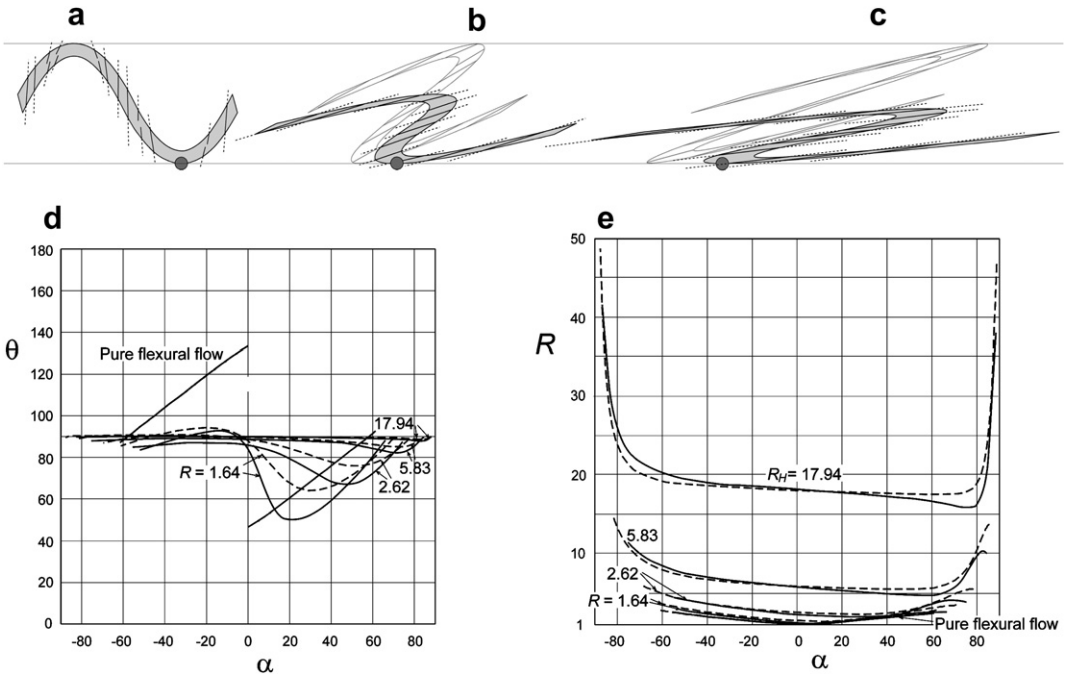

Fig. 5. a) Flexural flow fold with a parabolic guideline and aspect ratio $h = 1$. Lines intersecting the fold profile are trajectories of the maximum finite elongation. b) and c) The dark gray folds are numerical folds obtained with 'FoldModeler' for a simultaneous superimposition of simple shear and pure shear with a vertical maximum shortening direction on the fold in (a). R of the pure shear component ($R = k_1/k_2$) is equal to the square root of the axis ratio R_H of the strain ellipse of the total homogeneous strain. The dark circles show the migration of the hinge zone of the initial fold along the backlimb with progressive shearing. R_H is 5.83 in (b) and 17.54 in (c). These values correspond to the R-values for $\gamma = 2$ and $\gamma = 4$, respectively. Folds corresponding to the superimposition of simple shear deformation with $\gamma = 2$ and $\gamma = 4$ on the fold in (a) are shown in a light gray pattern to allow comparison. d) Black curves are θ–α curves for the initial fold and the folds formed by simultaneous superimposition of pure shear and simple shear. R_H is shown on the curves. ϕ–α curves for folds formed by a superimposition of simple shear with the same R_H value are shown in gray to allow comparison. e) Black curves are R–α curves for the initial fold and the folds formed by simultaneous superimposition of pure shear and simple shear. R–α curves for folds formed by a superimposition of simple shear with the same R_H value are shown with a dashed line to allow comparison. R_H is shown on the curves.

zone than in the rest of the hinge zone, the existence of a bulge in this inner, etc.).

An important problem for this modelling is that the fold attitude prior to the superimposition of the homogeneous deformation is not known in nature. For an asymmetric fold formed by a combination of layer parallel shortening, TLS and/or FF plus a superimposed homogeneous deformation, although the final position of the fold is known, there are infinite sequences of kinematic mechanisms that can fit the fold. These sequences produce the same strain ellipse and the same final geometry; they only differ in the rotational component. Hence, they correspond to different initial positions of the fold prior to the deformation superimposition. Fortunately, all the possibilities are not equally probable and the homogeneous deformation more appropriate can be chosen in many cases from the analysis of field data. For example, we can suppose in most cases that the vergence is in the same direction during the whole development of the fold, and cases in which the vergence of the fold prior to the superimposition is opposite to the vergence of the final fold can be ignored.

The easiest fit of a natural fold with homogeneous superimposed deformation is using an irrotational strain. From this initial fitting, other fits are then sought from a deformation consisting of a combination of simple shear and irrotational strain. This analysis is based on the following fundamental theorem (Truesdell and Toupin, 1960, p. 274): The homogeneous deformation of a body may be regarded as resulting from a translation, a rigid rotation of the principal axes of strain, and stretches along these axes. Hence, in the analysis it is useful to consider a combination of simple shear and irrotational strain, with the shear direction of the simple shear component in coincidence with a principal direction of the irrotational strain component, as the product of an irrotational strain and a rigid rotation; i.e.:

$$r \circ f = g, \tag{4}$$

where r is the rotation, f is the material deformation gradient tensor of the irrotational strain, and g is the material deformation gradient tensor of the combination of simple shear and irrotational strain (with respect to a reference system with the x-axis in the shear direction of the simple shear component, g is given by the matrix (3)). If we determine the principal directions and values of the Green's strain tensor corresponding to f from the fit of the natural fold, determine the area change and assign values to k_1 in matrix (3), we can determine the rotation angle β, the γ value in matrix (3), and the angle θ that defines the shear direction of the simple shear component. A detailed analysis of equation (4) with the calculations to obtain the above parameters is given in Appendix C.

An example of fitting a natural fold using this method is shown in Fig. 7. The fold is located in the southern Pyrenees and developed in Eocene sandstones and mudstones in turbiditic facies; its axial plane dips 57° southwards. A good fit of this fold is obtained with a first folding step of isochoric layer parallel shortening ($\sqrt{\lambda_2} = 0.7$), a second step of ETLS with an aspect ratio of 0.67, and a third step of flattening (pure shear with $\sqrt{\lambda_2} = 0.84$) with a $\sqrt{\lambda_1}$-direction making an angle of −20° with the fold axial trace. However, this fold forms part of a long train of folds developed in the hanging wall of a major thrust (Gavarnie thrust) (Teixell, 1992). Folds and thrust verge southwards towards the foreland. Hence, this train probably resulted from a rotational bulk deformation regime. Assuming a regime of simple shear strain and using the equations deduced in Appendix C, the equivalent fit

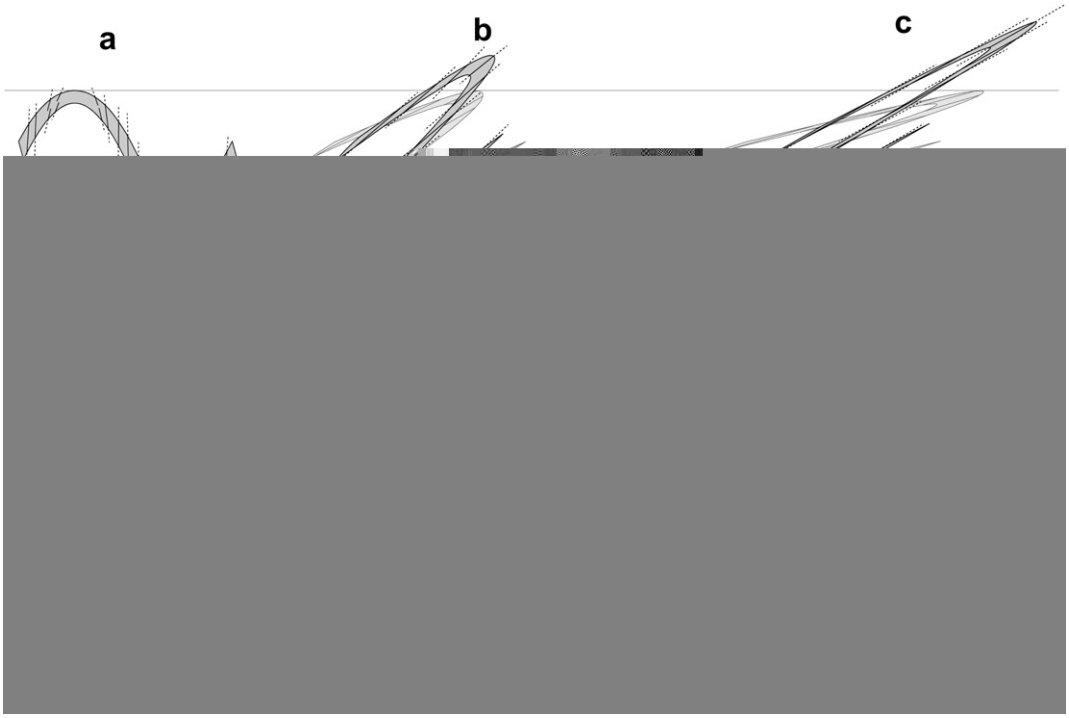

Fig. 6. a) Flexural flow fold with a parabolic guideline and aspect ratio $h = 1$. Lines intersecting the fold profile are trajectories of the maximum finite elongation. b) and c) The dark gray folds are numerical folds obtained with 'FoldModeler' for a simultaneous superimposition of simple shear and pure shear with a horizontal maximum shortening direction on the fold in (a). R of the pure shear component ($R = k_1/k_2$) is equal to the square root of the axis ratio R_H of the strain ellipse of the total homogeneous strain. The dark circles show the migration of the hinge zone of the initial fold along the backlimb with progressive shearing. R_H is 5.83 in (b) and 17.54 in (c). These values correspond to the R-values for $\gamma = 2$ and $\gamma = 4$, respectively. Folds corresponding to the superimposition of simple shear deformation with $\gamma = 2$ and $\gamma = 4$ on the fold in (a) are shown in a light gray pattern to allow comparison. d) Black curves are $\theta-\alpha$ curves for the initial fold and the folds formed by simultaneous superimposition of pure shear and simple shear. R_H is shown on the curves. $\theta-\alpha$ curves for folds formed by a superimposition of simple shear with the same R_H value are shown in gray to allow comparison. e) Black curves are $R-\alpha$ curves for the initial fold and the folds formed by simultaneous superimposition of pure shear and simple shear. $R-\alpha$ curves for folds formed by a superimposition of simple shear with the same R_H value are shown with a dashed line to allow comparison. R_H is shown on the curves.

involves a foreland-directed shear strain with $\gamma = 0.35$ and a shear direction plunging north 17°. Once the shear direction, the γ value and the present dip of the fold axial plane are known, the dip of the axial plane prior the superimposition of the simple shear can be determined; this dip was about 66° northwards and it could be produced, in a bulk simple shear regime, by buckling of layers oblique to the shear direction.

8. Application to recumbent folds

Large recumbent folds form an important feature of many orogenic belts, but their origin and development are not well understood. Several authors have explained or developed experimentally recumbent folds by buckling in a regime of simple shear (Ghosh, 1966; Ramsay et al., 1983; Sanderson, 1979; Ez, 2000; Carreras et al., 2005). This mechanism requires a high angle between the layers and the shear plane, involving in general a steep dip of the layers. It has been invoked to explain outcrop-scale folds, often related to ductile shear zones or thrusts (Sanderson, 1982; Rattey and Sanderson, 1982; Carreras et al., 2005). Ramsay et al. (1983) proposed the formation of large recumbent folds in the Helvetic nappes by this deformation type; these authors suggest that the folds formed in the frontal culmination wall of the nappe, where the layers had reached a substantial dip before the development of the recumbent folds. On the other hand, Dietrich and Casey (1989) used a combination of simple shear and pure shear, with the latter decreasing towards the external parts of the belt, to explain the same folds. Treagus (1999) also used a combination of simple shear and pure shear to explain the evolution of the Tay nappe in the Central Highlands of Scotland. Hudleston (1977), by observation of somewhat similar recumbent folds in glaciers, suggested that these structures can form by superimposition, under influence of gravity, of a homogeneous simple shear on prior gentle waves. This author also suggested that recumbent folds in orogenic belts may form in an analogous manner. Nonetheless, the folds obtained for this mechanism require a huge superposed strain to give rise to tight or isoclinal recumbent folds similar to those common in orogenic belts.

Simulation of recumbent folds with 'FoldModeler' permits the kinematic analysis of these interesting structures. Although a rotational deformation is necessary to explain the asymmetry and vergence of large recumbent folds, these are difficult to explain in a simple shear regime, because their development would require high original dip of the layers or huge strains. Nonetheless, the superimposition of a combination of simple shear and irrotational strain on pre-existing buckle folds can enhance the recumbent character of folds. A graphical representation of the axial surface dip against the major principal stretch is shown in Fig. 8 for simple shear and a simultaneous combination of simple shear and pure shear (sub-simple shear; De Paor, 1983; Simpson and De Paor, 1993), in which the major semi-axis of the strain ellipse of the pure shear component is the square root of the major semi-axis of the global strain ellipse. Each curve corresponds to a specific dip of the axial surface of the fold prior of the homogeneous strain superimposition. From this figure it is apparent that the development of a recumbent fold by superimposition of sub-simple shear on a buckle fold requires much less strain than by superimposition of simple shear. The modelled folds of Fig. 5 illustrate this assertion.

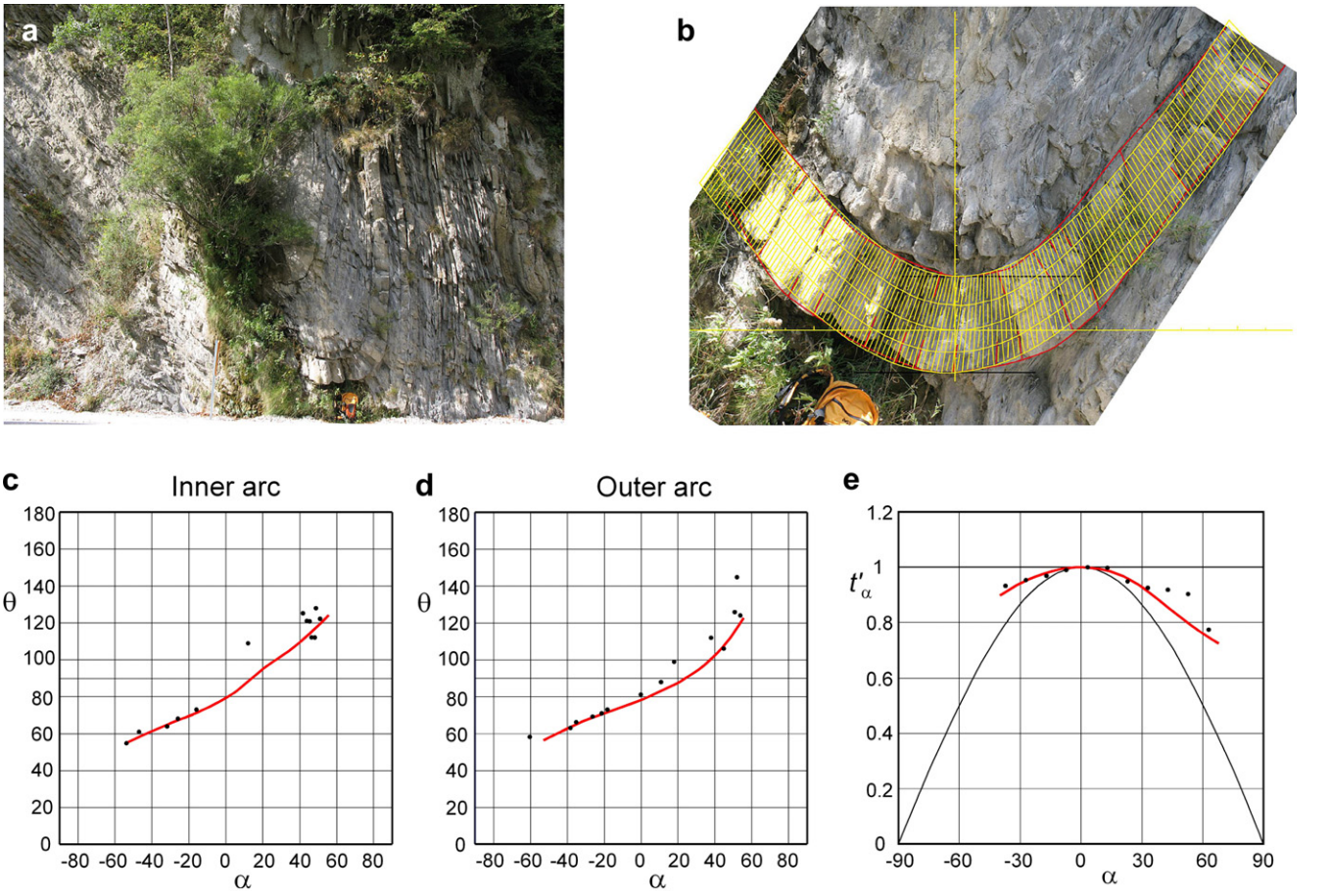

Fig. 7. Example of fit of a natural fold using 'FoldModeler'. a) Syncline developed in Eocene sandstones and lutites (near Isaba, Navarra, Spain; southern part of the western Pyrenees; looking to the west). b) Superimposition of the theoretical fold on the natural fold. The fold has been rotated to have its coordinate axes superposed on those of the numerical fold. Details of the modelling are given in the text. c) and d) Comparison of $\theta-\alpha$ curves for the numerical fold (red line) with the data of the natural fold (black points). e) Comparison of the Ramsay's classification for the theoretical (red line) and the natural fold (black points).(For interpretation of the references to colour in this figure legend, the reader is referred to the web version of this article.)

The kinematic modelling of recumbent folds suggests that their development involves the following requirements: a) a tectonic regime with a rotational bulk deformation with sub-horizontal simple shear components inducing buckling in a multilayer dipping in the same sense as the shear direction; b) superimposition of a deformation of homogeneous tendency consisting of a combination of simple shear, with a sub-horizontal shear direction, and irrotational strain, with a sub-vertical direction of maximum shortening. The irrotational strain component must increase with time during the complete process, since in the stage a) this component would prevent the buckling, except in cases with very high initial dip, and the absence of irrotational strain in the stage b) would prevent the development of recumbent folds except in cases with very high dip or strain. A consequence of this mechanism is the appearance of an extensional sub-horizontal deformation. The irrotational strain component can increase with the fold development as a consequence of the increasing influence of the gravity with the tectonic superimposition associated with the fold development. This evolutionary model has been used to explain the development of the recumbent fold of the Courel (Variscan belt, NW Spain), in which the existence of components of irrotational strain with sub-vertical maximum shortening allowed (Fernández et al., 2007) to explain the presence of a stretching lineation in the axial direction of the fold. This lineation cannot be explained only by simple shear with shear direction perpendicular to the axial direction.

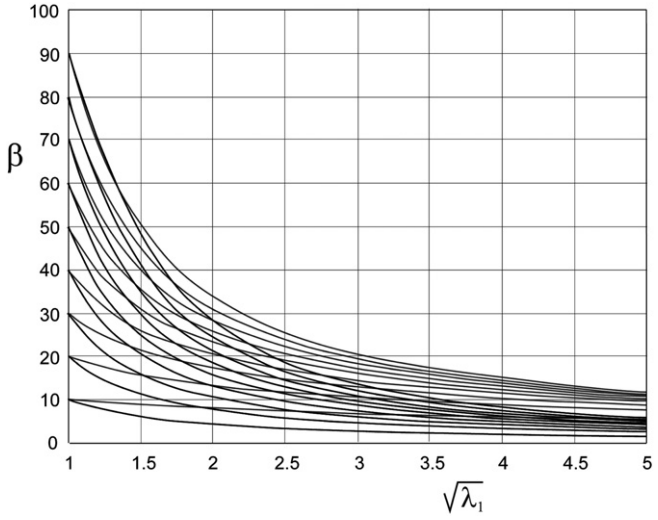

Fig. 8. Variation of the axial surface dip (β) of a fold against the major principal stretch ($\sqrt{\lambda_1}$) for simple shear (gray curves) and for a simultaneous combination of pure shear and simple shear in which the major semi-axis of the strain ellipse of the pure shear component is the square root of the major semi-axis of the global strain ellipse (black curves).

9. Discussion and conclusions

Determining the kinematic mechanisms that gave rise to a specific fold is a difficult problem because we only can know the final result of the deformation process. Therefore, attention must be paid to any feature that gives clues regarding the history of the deformation, especially the cleavage distribution. Unfortunately, these indications are often insufficient to determine the strain state inside the folded layers and the kinematic mechanisms that gave rise to the folding. Therefore, it is necessary to construct mathematical or experimental models or simulations that can shed light on the rules of folding development. Mathematical analysis of folding kinematics has allowed us constructing a new version or the 'FoldModeler' software that can be used for the forward or inverse modelling of asymmetric folds.

In the forward modelling, there are countless possible combinations of kinematic mechanisms that are capable of producing asymmetric folds. Experimental studies suggest that the fold asymmetry induced during buckling is not large, even in a non-coaxial bulk deformation context (Ghosh, 1966; Anthony and Wickham, 1978; Manz and Wickham, 1978; Carreras et al., 2005). Therefore, the main source of asymmetry must be produced during the kinematic amplification due to the superimposition of a homogeneous or nearly homogeneous strain with the direction of maximum finite stretch oblique to the axial trace. Hinge point migration is an important consequence of this deformation that strongly influences the strain distribution in the folded layer. Simple shear or a combination of simple shear and irrotational strain, with a principal direction coincident with the shear direction, seem to be common deformations superposed on active folding in natural asymmetric folds (Sanderson, 1979, 1982; Ramsay, 1980; Ramsay et al., 1983; Ridley and Casey, 1989; Casey and Dietrich, 1997; Treagus, 1999; Harris et al., 2002; Alsop and Carreras, 2007). In both cases, if the pre-existing buckle folds are parallel, the resulting fold is class 1C, comparable to the folds formed by symmetric flattening, although with different relative length of limbs and a thickness asymmetry. In general, for the same final superposed strain, folds formed by a simultaneous combination of simple shear and irrotational strain, with the maximum shortening perpendicular to the shear direction, have a gentler dipping axial plane and a thicker forelimb than those formed by simple shear or by a simultaneous combination of simple shear and irrotational strain with the maximum shortening along the shear direction.

In the inverse modelling, a specific natural fold can be fitted by folds formed by infinite combinations of kinematic mechanisms, which produce the same final form and only differ in the rotational component. Regional geological constraints, like the fold vergence or the deformation regime, or vorticity gauges (e.g., quartz fabrics measured around a fold) can restrict the number of possible fits. The fact that a rotational deformation composed of a simultaneous combination of simple shear and pure shear can be analytically obtained as result of an irrotational strain plus a rigid rotation allows establishing an equation whose analysis makes the fitting easier.

Application of the 'FoldModeler' software to understanding large recumbent folds suggests some interesting conclusions. Development of these folds requires a rotational deformation regime with a sub-horizontal simple shear component. The original layering must be oblique to the shear direction and must have an initial dip direction in the shear direction. Under these conditions, a buckle fold must be developed under the rotational regime. This fold must subsequently undergo a kinematic amplification as a consequence of the superimposition of a combination of simple shear and irrotational strain, which is probably a sub-simple shear in many cases. Superimposition of an irrotational strain component at this stage allows the development of recumbent folds with application of much less strain than with superimposition of simple shear only. The amount of the irrotational strain component probably increases with the development of the fold due to an increasing influence of gravity as a consequence of the tectonic superimposition of rocks.

Kinematic models of folding developed numerically by computer are obviously simple approaches to the complexity of the geological reality. The models used here are 2D geometrical models developed in a single layer, not considering therefore the complex kinematic mechanisms derived from the mechanical anisotropies and heterogeneities of a multilayer or thermal heterogeneities as those considered by Bucher (1956). The models do not incorporate the effects of the existence of fractures or other elements either, such as blocks that can act as a buttress to enhance the folding and favour the development of recumbent folds (Bucher, 1956, 1962; Vacas Peña and Martínez Catalán, 2004). Despite the limitations of the mathematical models and of the folds produced numerically with 'FoldModeler', this program allows forward and inverse modelling, and due to its analytical character, it allows analysis of the deformation components that give rise to a specific numerical or a natural fold. In addition, this program also allows a geometrical-kinematic basis to be established for the subsequent mechanical modelling of folds.

Acknowledgements

The present work was supported by Spanish CGL2008-03786/BTE project funded by Ministerio de Ciencia e Innovación and Fondo Europeo de Desarrollo Regional (FEDER) and the project 'Topo-Iberia' (CSD2006-0041) of the Spanish CONSOLIDER-INGENIO 2010 Program. We are grateful to J. Poblet, D.C. Srivastava and S.H. Treagus for many valuable suggestions that notably improved the manuscript.

Appendix A. Material deformation gradient of simultaneous simple shear and irrotational strain

To represent analytically the simultaneous effect of an irrotational strain and a simple shear, we consider an elemental transformation with matrix:

$$\tilde{M} = \tilde{B}\tilde{A}, \quad \tilde{A} = \begin{pmatrix} 1+\tilde{a} & 0 \\ 0 & 1+\tilde{b} \end{pmatrix}, \quad \tilde{B} = \begin{pmatrix} 1 & \tilde{\gamma} \\ 0 & 1 \end{pmatrix}. \tag{A-1}$$

This transformation is iterated a very large number of times. So, we obtain the matrix G:

$$G = \lim_{n\to\infty} \left(\tilde{M}\right)^n \tag{A-2}$$

When n tends to infinity, the matrix $\tilde{M} = \tilde{B}\tilde{A}$ must be close to the unit matrix for the matrix G to be finite. In other words, the matrices $\tilde{A}$ and $\tilde{B}$ must be of the form:

$$\tilde{A} = \begin{pmatrix} 1+a_n & 0 \\ 0 & 1+b_n \end{pmatrix}, \quad \tilde{B} = \begin{pmatrix} 1 & \gamma_n \\ 0 & 1 \end{pmatrix}, \tag{A-3}$$

where

$$\lim_{n\to\infty} a_n = 0, \quad \lim_{n\to\infty} b_n = 0, \quad \lim_{n\to\infty} \gamma_n = 0. \tag{A-4}$$

More specifically, the limits

$$\lim_{n\to\infty} na_n, \quad \lim_{n\to\infty} nb_n, \quad \lim_{n\to\infty} n\gamma_n \tag{A-5}$$

have to be finite. Without loss of generality, we can write:

$$a_n = \frac{a}{n}, \quad b_n = \frac{b}{n}, \quad \gamma_n = \frac{\gamma}{n}. \tag{A-6}$$

Now, the matrices $\tilde{A}$ and $\tilde{B}$ become:

$$\tilde{A} = I + \frac{1}{n}A, \quad \tilde{B} = I + \frac{1}{n}B \tag{A-7}$$

With

$$A = \begin{pmatrix} a & 0 \\ 0 & b \end{pmatrix}, \quad B = \begin{pmatrix} 1 & \gamma \\ 0 & 1 \end{pmatrix}. \tag{A-8}$$

Then, the elementary deformation is:

$$\tilde{M} = \left(I + \frac{1}{n}B\right)\left(I + \frac{1}{n}A\right) = I + \frac{1}{n}(A+B) + \frac{1}{n^2}BA. \tag{A-9}$$

The non-commutative part of this product, i.e., the term BA, is preceded by the factor $1/n^2$, which is smaller than the commutative part $(A + B)/n$, and it does not affect the value of the power $\tilde{M}_n$ when $n \to \infty$. Hence, we have the following equation for the matrix G:

$$G = \lim_{n\to\infty}\left(I + \frac{1}{n}C\right)^n, \quad \text{where } C = A + B. \tag{A-10}$$

The last equation of G coincides with the usual definition of the exponential of a matrix:

$$\exp C := \lim_{n\to\infty}\left(I + \frac{1}{n}C\right)^n, \quad G = \exp C, \quad C = \begin{pmatrix} a & \gamma \\ 0 & b \end{pmatrix}. \tag{A-11}$$

This results synthesizes analytically the geometrical idea of infinitely small infinite transformations. Matrix C is diagonalizable and it can be exponentiated without difficulty. The result is (Moler and Van Loan, 1978):

$$G = \begin{pmatrix} k_1 & \gamma\frac{k_1-k_2}{\ln(k_1/k_2)} \\ 0 & k_2 \end{pmatrix}, \quad k_1 = \exp a, \quad k_2 = \exp b. \tag{A-12}$$

Appendix B. Coordinate change associated to a migration of the hinge point

In the coordinate system $\{O,B\}$, with origin O and basis of orthonormal basis $B = (\hat{\mathbf{E}}_1, \hat{\mathbf{E}}_2)$ (Fig. B-1a), the conic section that describes the guideline before the homogeneous strain has the equation:

$$R^T G R - 2KR = 0, \tag{B-1}$$

where

$$G = \begin{pmatrix} 1 & 0 \\ 0 & 1 - E^2 \end{pmatrix}, \quad \text{quadratic form matrix}, \tag{B-2}$$

$$R = \begin{pmatrix} X \\ Y \end{pmatrix}, \quad \text{matrix}, \tag{B-3}$$

$$K = \begin{pmatrix} 0 & A \end{pmatrix}, \quad \text{linear form matrix}. \tag{B-4}$$

Here, E is the eccentricity and A the scale factor.

Let us consider now the homogeneous strain given by:

$$R = HR', \tag{B-5}$$

where R' is the matrix of the coordinates of the deformed point, and H^{-1} is the spatial deformation gradient matrix. The equation of the deformed guideline, also a conic, in the same coordinate system B, is

$$R'TG'R' - 2K'R' = 0, \tag{B-6}$$

with $G' = H^T G H$ and $K' = KH$.

Let us consider now a new orthonormal basis $b = (\mathbf{e}_1, \mathbf{e}_2)$ (Fig. B-1b). In the new coordinate system $\{O,b\}$ the deformed conic has the equation:

$$\tilde{R}^T \tilde{G}_0 \tilde{R} - 2\tilde{K}_0 \tilde{R} = 0, \tag{B-7}$$

where $\tilde{G}_0 = P^T G' P$, $\tilde{K}_0 = K'P$, $R' = P\tilde{R}$, and P is the base change matrix.

We choose the new base b formed by the orthonormal eigenvectors of G', so $\tilde{G}_0$ is a diagonal matrix

$$\tilde{G}_0 = \begin{pmatrix} g_1 & 0 \\ 0 & g_2 \end{pmatrix}, \quad \text{with } g_1 > g_2, \tag{B-8}$$

The quotient g_2/g_1 is related to the eccentricity of the deformed guideline:

$$e = \sqrt{1 - g_2/g_1}. \tag{B-9}$$

Making $\tilde{G} = \tilde{G}_0/g_1$ and $\tilde{K} = \tilde{K}_0/g_1$, we obtain from (A-7)

$$\tilde{R}^T \tilde{G} \tilde{R} - 2\tilde{K}\tilde{R} = 0. \tag{B-10}$$

To obtain the linear part in equation (B-10) in the simple form in equation (B-4), we change the coordinate origin, so the new origin o, with position vector R_o (Fig. B-1b), coincides with the hinge point of the deformed guideline. Then, the new position vector $\overline{R}$ of a point of the deformed guideline is related to the old vector $\tilde{R}$ by

$$\tilde{R} = R_o + \overline{R}. \tag{B-11}$$

Introducing this equation in (B-10), we obtain

$$\overline{R}^T \tilde{G} \overline{R} - 2\left(\tilde{K} - R_o^T \tilde{G}\right)\overline{R} = 0, \tag{B-12}$$

where R_o must satisfy equation (B-10), that is,

$$R_o \tilde{G} R_o - 2\tilde{K} R_o = 0. \tag{B-13}$$

The minuend in equation (B-12) has the same form of the one in equation (B-1). Let us force that the subtrahend in both equations has the same form, that is,

$$\tilde{K} - R_o^T \tilde{G} = \begin{pmatrix} 0 & a \end{pmatrix}, \tag{B-14}$$

where a is the new scale factor.

Equations (B-13) and (B-14) form a system of three scalar equations that allows to obtain R_o and a. Solving it, we have

$$x_0 = \tilde{K}_1, \tag{B-15}$$

$$y_0 = \frac{g_1\tilde{K}_2 - \sqrt{g_1^2\tilde{K}_2^2 + g_1 g_2 \tilde{K}_1^2}}{g_2}, \tag{B-16}$$

$$a = \tilde{K}_2 - y_0\frac{g_2}{g_1}, \tag{B-17}$$

where $\tilde{K} = \begin{pmatrix} \tilde{K}_1 & \tilde{K}_2 \end{pmatrix}$ and

$$R_o = \begin{pmatrix} x_0 \\ y_0 \end{pmatrix}.$$

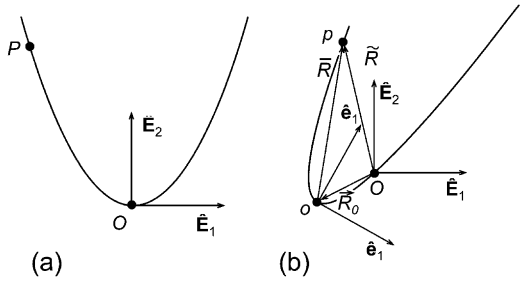

Fig. B-1. Coordinate change associated with hinge migration due to superimposition of a general homogeneous strain on a pre-existing fold.

Appendix C. Analysis of equation (4) ($r \circ f = g$)

1. Preliminary definitions and notation

Let $b = (\hat{\mathbf{e}}_1, \hat{\mathbf{e}}_2)$ be an orthonormal basis defined in a fold (Fig. C-1a). An orthonormal basis rotated an angle z with respect to the basis b (Fig. C-1b) is designated by

$$b^z = \left(\hat{\mathbf{e}}_1^z, \hat{\mathbf{e}}_2^z\right).$$

We can observe that $b^0 = b$.

Let us define an irrotational strain gradient, f, in the directions of the basis b^α. Its matrix F in the basis b^α is:

$$F = (f)_{b^\alpha} = \begin{pmatrix} l & 0 \\ 0 & m \end{pmatrix}, \tag{C-1}$$

where the symbol $(f)_{b^\alpha}$ represents the matrix of the lineal operator f in the basis b^α.

Let g be the gradient of a simultaneous superimposition of simple shear and irrotational strain in the directions of the basis b^θ. Accordingly with Appendix A, its matrix is:

$$G = (g)_{b^\theta} = \begin{pmatrix} k_1 & \gamma\frac{k_1-k_2}{\ln(k_1/k_2)} \\ 0 & k_2 \end{pmatrix}. \tag{C-2}$$

Let r be the gradient of a rotation defined by angle β. Its matrix R is independent of the considered orthonormal basis.

$$R = (r)_{\cdot} = \begin{pmatrix} \cos\beta & -\sin\beta \\ \sin\beta & \cos\beta \end{pmatrix}. \tag{C-3}$$

2. Approach to the problem

We must analyse under what conditions we can factorize the gradient g, defined in (C-2), with parameters θ, k_1, k_2 and γ, as a product of the rotation r, with parameter β, and the irrotational strain f, with parameters α, l and m. In other words, we want to know how the parameters $\theta, k_1, k_2, \gamma, \beta, \alpha, l$ and m are related, so that the following composition relation is accomplished:

$$r \circ f = g. \tag{C-4}$$

This operational equation becomes a matrix equation when we choose a specific vector basis. Taking the basis b^α, we have

$$(r)_{b^\alpha}(f)_{b^\alpha} = (g)_{b^\alpha}. \tag{C-5}$$

In agreement with definitions (C-1) and (C-3), the left-hand side is the matrix

$$L = RF, \tag{C-6}$$

$$L = \begin{pmatrix} l\cos\beta & -m\sin\beta \\ l\sin\beta & m\cos\beta \end{pmatrix}. \tag{C-7}$$

For the matrix of the second member of (C-5) we have:

$$(g)_{b^\alpha} = Q^T(g)_{b^\theta}Q = Q^T G Q, \tag{C-8}$$

where Q is the matrix of basis change,

$$Q = \begin{pmatrix} \cos\theta' & \sin\theta' \\ -\sin\theta' & \cos\theta' \end{pmatrix}, \quad \theta' = \theta - \alpha. \tag{C-9}$$

Now the equation (C-5) has the form

$$L = Q^T G Q. \tag{C-10}$$

Be h the area change of the transformation g:

$$h = \det g = \det G = k_1 k_2.$$

Taking into account equation (C-10), we also have:

$$h = \det(rf) = (\det r)(\det f) = 1 \det F = lm.$$

Hence, we have the double relation

$$lm = k_1 k_2 = h. \tag{C-11}$$

3. Some necessary conditions

Equation (C-10) shows that L and G are similar matrices and therefore they have the same characteristic polynomial. If we identify the corresponding equations:

$$(L) \quad \lambda^2 - \left(l + \frac{h}{l}\right)\cos\beta\lambda + h = 0, \tag{C-12}$$

$$(G) \quad \lambda^2 - (k_1 + k_2)\lambda + h = 0, \tag{C-13}$$

We obtain the relation:

$$\left(l + \frac{h}{l}\right)\cos\beta = k_1 + k_2 = 2\omega. \tag{C-14}$$

The eigenvalues, common for the two matrices, are:

$$\lambda_1 = \omega + \sqrt{\omega^2 - h}, \quad \lambda_2 = \omega - \sqrt{\omega^2 - h}. \tag{C-15}$$

For the *normal case*, $\omega > \sqrt{h}$, we have $\lambda_1 \neq \lambda_2$, but for the *degenerate case*, $\omega = \sqrt{h}$, $\lambda_1 = \lambda_2$.

In an analogous way, as the matrices F^TF and G^TG are similar,

$$G^TG = Q\left(F^TF\right)Q^T,$$

their characteristic equations:

$$\left(F^TF\right) \quad \lambda^2 - \left(l^2 + \frac{h^2}{l^2}\right)\lambda + h^2 = 0, \tag{C-16}$$

$$\left(G^TG\right) \quad \lambda^2 - \left(k_1^2 + k_2^2 + \left(\gamma\frac{k_1 - k_2}{\ln(k_1/k_2)}\right)^2\right)\lambda + h^2 = 0, \tag{C-17}$$

must be identical. Hence, we have the relation:

$$l^2 + \frac{h^2}{l^2} = k_1^2 + k_2^2 + \left(\gamma \frac{k_1 - k_2}{\ln(k_1/k_2)}\right)^2. \quad \text{(C-18)}$$

The eigenvectors of L, of matrices V_i ($i = 1, 2$), verify

$$LV_i = \lambda_i V_i, \quad \text{(C-19)}$$

where the λ_i have been defined in (C-12). From (C-19) we obtain:

$$V_i = \begin{pmatrix} A_i \\ B_i \end{pmatrix}, \quad \begin{cases} A_i = h\sin\beta \\ B_i = l(l\cos\beta - \lambda_i) \end{cases}, \quad \text{(C-20)}$$

The eigenvectors W_i of G,

$$GW_i = \lambda_i W_i, \quad i = 1, 2, \quad \text{(C-21)}$$

are:

$$W_i = QV_i, \quad \text{(C-22)}$$

From (C-20) we have:

$$W_i = \begin{pmatrix} C_i \\ D_i \end{pmatrix}, \quad \begin{cases} C_i = A_i\cos\theta' + B_i\sin\theta', \\ D_i = -A_i\sin\theta' + B_i\cos\theta' \end{cases}. \quad \text{(C-23)}$$

4. Sufficient conditions

Here we will obtain the conditions that the parameters of the transformations must accomplish to satisfy the fundamental relation (C-4).

We assume in this section that $\omega > \sqrt{h}$ (normal case). Since the eigenvalues are different, the associated eigenvectors, and their matrices V_1 and V_2, are linearly independent. In these conditions, the matrix equality (C-10) is equivalent to the two vector relations:

$$Q^T G Q V_i = LV_i, \quad i = 1, 2. \quad \text{(C-24)}$$

Using the notation (C-23), equation (C-21) takes the form:

$$\begin{pmatrix} k_1 & \gamma\frac{k_1 - k_2}{\ln k_1 - \ln k_2} \\ 0 & k_2 \end{pmatrix} \begin{pmatrix} C_i \\ D_i \end{pmatrix} = \lambda_i \begin{pmatrix} C_i \\ D_i \end{pmatrix}. \quad \text{(C-25)}$$

From this equation, we obtain the relations searched:

$$\lambda_i = k_i, \quad i = 1, 2, \quad \text{(C-26)}$$

$$\tan\theta' = \frac{l(l\cos\beta - k_1)}{h\sin\beta}, \quad \text{(C-27)}$$

$$\gamma = \frac{\cos(\theta' - \varepsilon)}{\sin(\theta' - \varepsilon)} \ln\frac{k_1}{k_2}, \quad \text{(C-28)}$$

where

$$\tan\varepsilon = \frac{l(l\cos\beta - k_2)}{h\sin\beta}. \quad \text{(C-29)}$$

5. Degenerate case

In agreement with equation (C-15), for the case $\omega = \sqrt{h}$, we have:

$$\lambda_1 = \lambda_2 = \sqrt{h}, \quad \text{(C-30)}$$

$$k_1 = k_2 = k = \sqrt{h}, \quad \text{(C-31)}$$

$$G = \lim_{k_2 \to k_1} \begin{pmatrix} k_1 & \gamma\frac{k_1 - k_2}{\ln k_1 - \ln k_2} \\ 0 & k_2 \end{pmatrix} = k \begin{pmatrix} 1 & \gamma \\ 0 & 1 \end{pmatrix}. \quad \text{(C-32)}$$

The rotation angle β is determined from equation (C-14):

$$\cos\beta = \frac{2\sqrt{h}}{l + \frac{h}{l}}. \quad \text{(C-33)}$$

The system (C-16) takes now the form:

$$\sqrt{h}\begin{pmatrix} 1 & \gamma \\ 0 & 1 \end{pmatrix}\begin{pmatrix} C_i \\ D_i \end{pmatrix} = \sqrt{h}\begin{pmatrix} C_i \\ D_i \end{pmatrix}.$$

From this equation we obtain: $\theta = \theta' + \alpha$,

$$\tan\theta' = \frac{l\left(l\cos\beta - \sqrt{h}\right)}{h\sin\beta} \quad \text{(C-34)}$$

The value of γ is obtained from the matrix G, which can be found from equation (C-10),

$$G = QRFQ^T. \quad \text{(C-35)}$$

This choice of G guarantees the fulfillment of equation (C-4).

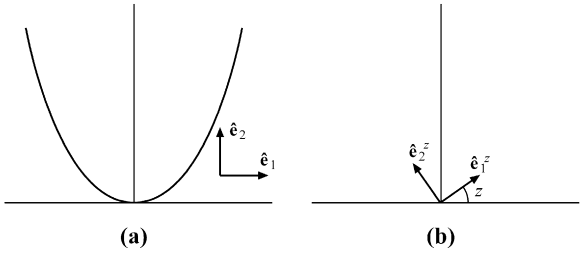

Fig. C-1. (a) Orthonormal basis, $b = (\hat{\mathbf{e}}_1, \hat{\mathbf{e}}_2)$, defined in a fold. (b) Orthonormal basis, $b^z = (\hat{\mathbf{e}}_1^z, \hat{\mathbf{e}}_2^z)$, rotated an angle z with respect to the basis defined in the fold.

References

Aller, J., Bastida, F., Toimil, N.C., Bobillo-Ares, N.C., 2004. The use of conic sections for the geometrical analysis of folded surface profiles. Tectonophysics 379, 239–254.

Alsop, G.I., Carreras, J., 2007. The structural evolution of sheath folds: a study case from Cap de Creus. Journal of Structural Geology 29, 1915–1930.

Anthony, M., Wickham, J., 1978. Finite-element simulation of asymmetric folding. Tectonophysics 47, 1–14.

Bastida, F., Aller, J., Bobillo-Ares, N.C., 1999. Geometrical analysis of folded surfaces using simple functions. Journal of Structural Geology 21, 729–742.

Bastida, F., Aller, J., Bobillo-Ares, N.C., Toimil, N.C., 2005. Fold geometry: a basis for their kinematical analysis. Earth-Science Reviews 70, 129–164.

Bastida, F., Aller, J., Toimil, N.C., Lisle, R.J., Bobillo-Ares, N.C., 2007. Some considerations on the kinematics of chevron folds. Journal of Structural Geology 29, 1185–1200.

Bastida, F., Bobillo-Ares, N.C., Aller, J., Toimil, N.C., 2003. Analysis of folding by superposition of strain patterns. Journal of Structural Geology 25, 1121–1139.

Biot, M.A., 1961. Theory of folding of stratified visco-elastic media and its implications in tectonics and orogenesis. Geological Society of America Bulletin 75, 563–568.

Bobillo-Ares, N.C., Aller, J., Bastida, F., Lisle, R.J., Toimil, N.C., 2006. The problem of area change in tangential longitudinal strain folding. Journal of Structural Geology 28, 1835–1848.

Bobillo-Ares, N.C., Bastida, F., Aller, J., 2000. On tangential longitudinal strain folding. Tectonophysics 319, 53–68.

Bobillo-Ares, N.C., Toimil, N.C., Aller, J., Bastida, F., 2004. "FoldModeler": a tool for the geometrical and kinematical analysis of folds. Computers & Geosciences 30, 147–159.

Brannan, D.A., Esplen, M.F., Gray, J.J., 1999. Geometry. Cambridge University Press, Cambridge.

Bucher, W.H., 1956. Role of gravity in orogenesis. Bulletin of the Geological Society of America 67, 1295–1318.
Bucher, W.H., 1962. An experiment on the role of gravity in orogenic folding. Geologische Rundschau 52, 804–810.
Carreras, J., Druget, E., Griera, A., 2005. Shear zone-related folds. Journal of Structural Geology 27, 1229–1251.
Casey, M., Dietrich, D., 1997. Overthrust shear in mountain building. In: Sengupta, S. (Ed.), Evolution of Geological Structures in Micro- to Macro-scales. Chapman & Hall, London, pp. 119–142.
Cobbold, P.R., Quinquis, H., 1980. Development of sheath folds in shear regimes. Journal of Structural Geology 2, 119–126.
Currie, J.B., Patnode, H.W., Trump, R.P., 1962. Development of folds in sedimentary strata. Geological Society of America Bulletin 73, 655–674.
De Paor, D.G., 1983. Orthographic analysis of geological structures-I. Deformation theory. Journal of Structural Geology 5, 255–278.
De Sitter, L.U., 1964. Structural Geology, second ed. McGraw-Hill, New York.
Dietrich, D., Casey, M., 1989. A new tectonic model for the Helvetic mappes. In: Coward, M.P., Dietrich, D., Park, R.G. (Eds.), Alpine Tectonics. Geological Society of London Special Publication, vol. 45, pp. 47–63.
Donath, F.A., 1963. Fundamental problems in dynamic structural geology. In: Donnelly, T.W. (Ed.), The Earth Sciences. William Marsh Rice University, Chicago & London, pp. 83–103.
Donath, F.A., Parker, R.B., 1964. Folds and folding. Geological Society of America Bulletin 75, 45–62.
Ez, V., 2000. When shearing is a cause of folding. Earth-Science Reviews 51, 155–172.
Fernández, F.J., Aller, J., Bastida, F., 2007. Kinematics of a kilometric recumbent fold: the Courel syncline (Iberian massif, NW Spain). Journal of Structural Geology 29, 1650–1664.
Fisher, D.M., Anastasio, D.J., 1994. Kinematic analysis of a large-scale leading edge fold, Lost River Range, Idaho. Journal of Structural Geology 16, 337–354.
Fossen, H., Tikoff, B., 1993. The deformation matrix for simultaneous simple shearing, pure shearing, and volume change, and its application to transpression/transtension tectonics. Journal of Structural Geology 15, 413–422.
Frehner, M., Schmalholz, S.M., 2006. Numerical simulations of parasitic folding in multilayers. Journal of Structural Geology 28, 1647–1657.
Geiser, J., Geiser, P.A., Kligfield, R., Ratliff, R., Rowan, M., 1988. New applications of computer-based section construction: strain analysis, local balancing, and subsurface fault prediction. Mountain Geology 25, 47–59.
Ghosh, S.K., 1966. Experimental tests of buckling folds in relation to strain ellipsoid in simple shear deformation. Tectonophysics 3, 169–185.
Harris, L.B., Koyi, H.A., Fossen, H., 2002. Mechanisms for folding of high-grade rocks in extensional tectonic settings. Earth-Science Reviews 59, 163–210.
Hudleston, P.J., 1973. Fold morphology and some geometrical implications of theories of fold development. Tectonophysics 16, 1–46.
Hudleston, P.J., 1977. Similar folds, recumbent folds, and gravity tectonics in ice and rocks. Journal of Geology 85, 113–122.
Hudleston, P.J., Holst, T.B., 1984. Strain analysis in buckle folds and implications for the rheology of the layers during folding. Journal of Structural Geology 106, 321–347.
Hudleston, P.J., Srivastava, H.B., 1997. Strain and crystallographic fabric pattern in a folded calcite vein: the dependence on initial fabric. In: Sengupta, S. (Ed.), Evolution of Geological Structures in Micro- a Maroscales. Chapman & Hall, London, pp. 259–271.
Hudleston, P.J., Tabor, J.R., 1988. Strain and fabric development in a buckled calcite vein and rheological implications. Bulletin of the Geological Institute, University of Uppsala 14, 79–94.
Hudleston, P.J., Treagus, S., Lan, L., 1996. Flexural flow: does it occur in nature? Geology 24, 203–206.
Ickes, E.L., 1923. Similar, parallel and neutral surface types of folding. Economic Geology 18, 575–591.
Kuenen, P.U., de Sitter, L.U., 1938. Experimental investigation into the mechanism of folding. Leidse Geologische Mededelingen 10, 217–240.
Lisle, R.J., Fernández Martínez, J.L., Bobillo-Ares, N.C., Menéndez, O., Aller, J., Bastida, F., 2006. FOLD PROFILER: a MATLAB®-based program for fold shape classification. Computers & Geosciences 32, 102–108.
Lisle, R.J., Aller, J., Bastida, F., Bobillo-Ares, N.C., Toimil, N.C., 2009. Volumetric strains in neutral surface folding. Terra Nova 21, 14–20.
Loudon, T.V., 1964. Computer Analysis of Orientation Data in Structural Geology. Technical Report. Geography Branch Office of Naval Research, O.N.R. Task No. 389-135, Contr. No. 1228, No. 13, pp. 1–130.
Manz, R., Wickham, J., 1978. Experimental analysis of folding in simple shear. Tectonophysics 44, 79–90.
Merle, O., 1994. Nappes et chevauchments. Masson, Paris.
Moler, C., Van Loan, C., 1978. Nineteen dubious ways to compute the exponential of a matrix, twenty-five years. SIAM Review 20, 801–836.
Mukhopadhyay, D., 1965. Effects of compression on concentric folds and mechanism of similar folding. Journal of the Geological Society of India 6, 27–41.
Ormand, C.J., Hudleston, P.J., 2003. Strain paths of three small folds from the Appalachian Valley and Ridge, Maryland. Journal of Structural Geology 25, 1841–1854.
Passchier, C.W., Trouw, R.A.J., 2005. Microtectonics, second ed. Springer, Berlin, 366 pp.
Price, N.J., 1967. The development of asymmetric buckle folds in non-metamorphosed sediments. Tectonophysics 4, 173–201.
Price, N.J., Cosgrove, J.W., 1990. Analysis of Geological Structures. Cambridge University Press, Great Britain.
Ramberg, H., 1960. Relationship between length of arc and thickness of ptygmatically folded veins. American Journal of Science 258, 36–46.
Ramberg, H., 1975. Particle paths, displacement and progressive strain application to rocks. Tectonophysics 28, 1–37.
Ramsay, J.G., 1962. The geometry and mechanics of formation of "similar" type folds. Journal of Geology 70, 309–327.
Ramsay, J.G., 1967. Folding and Fracturing of Rocks. McGraw-Hill, London.
Ramsay, J.G., 1974. Development of chevron folds. Bulletin of the Geological Society of America 85, 1741–1754.
Ramsay, J.G., 1980. Shear zone geometry: a review. Journal of Structural Geology 2, 83–89.
Ramsay, J.G., Huber, M.I., 1987. The Techniques of Modern Structural Geology. In: Folds and Fractures, vol. 2. Academic Press, London.
Ramsay, J.G., Casey, M., Kligfield, R., 1983. Role of shear in development of the Helvetic fold-thrust belt of Switzerland. Geology 11, 439–442.
Rattey, P.R., Sanderson, D.J., 1982. Patterns of folding within nappes and thrust sheets: examples from the Variscan of southwest England. Tectonophysics 88, 247–267.
Ridley, J., Casey, M., 1989. Numerical modelling of folding in rotational strain histories: strain regimen expected in thrust belts and shear zones. Geology 17, 875–878.
Sanderson, D.J., 1979. The transition from upright to recumbent folding in the Variscan fold belt of southwest England: a model based on the kinematics of simple shear. Journal of Structural Geology 1, 171–180.
Sanderson, D.J., 1982. Models of strain variation in nappes and thrust sheets: a review. Tectonophysics 88, 201–233.
Siddans, A.W.B., 1972. Slaty cleavage – a review of research since 1815. Earth-Science Reviews 8, 205–232.
Simpson, C., De Paor, D.G., 1993. Strain and kinematic analysis in general shear zones. Journal of Structural Geology 15, 1–20.
Smythe, D.K., 1971. Viscous theory of angular folding by flexural flow. Tectonophysics 12, 415–543.
Southwick, D.L., 1987. Bundled slaty cleavage in laminated argillite, North-Central Minnesota. Journal of Structural Geology 9, 985–993.
Srivastava, D.C., Srivastava, P., 1988. The modification of parallel folds by progressive shearing parallel to the axial plane. Tectonophysics 156, 167–173.
Teixell, A., 1992. Estructura alpina en la transversal de la terminación occidental de la Zona Axial pirenaica. Unpublished PhD, Universitat de Barcelona.
Tikoff, B., Fossen, H., 1993. Simultaneous pure and simple shear: the unified deformation matrix. Tectonophysics 217, 267–283.
Tikoff, B., Fossen, H., 1996. Visualization of deformation: computer applications for teaching. In: DePaor, D.G. (Ed.), Structural Geology and Personal Computers. Pergamon, Oxford, pp. 75–96.
Timoshenko, S., 1940. Strength of Materials, Part I. D. Van Nostrand Company, New York.
Toimil, N.C., Fernández, F.J., 2007. Kinematic analysis of symmetrical natural folds developed in competent layers. Journal of Structural Geology 29, 467–480.
Treagus, J.E., 1999. A structural reinterpretation of the tummel belt and a transpressional model for the evolution of the Tay nappe in the Central Highlands of Scotland. Geological Magazine 6, 643–660.
Treagus, S.H., 1973. Buckling stability of a viscous single-layer system, oblique to the principal compression. Tectonophysics 19, 271–289.
Treagus, S.H., 1982. A new isogon-cleavage classification and its application to natural and model fold studies. Geological Journal 17, 49–64.
Treagus, S.H., Fletcher, R.C., 2009. Controls of folding on different scales in multilayered rocks. Journal of Structural Geology 31, 1340–1349.
Tripathi, A., Gairola, V.K., 1999. Fold symmetry-a quantitative description. Journal of Structural Geology 21, 719–727.
Truesdell, C., Toupin, R., 1960. The classical field theories. In: Flügge, S. (Ed.), Encyclopedia of Physics, vol. III/1. Springer, Berlin, pp. 226–793.
Turner, F.J., Weiss, L.E., 1963. Structural Analysis of Metamorphic Tectonites. McGraw-Hill, New York.
Twiss, R.J., 1988. Description and classification of folds in single surfaces. Journal of Structural Geology 10, 607–626.
Vacas Peña, J.M., Martínez Catalán, J.R., 2004. A computer program for the simulation of folds of different sizes under the influence of gravity. Computers & Geosciences 30, 33–43.
Weijermars, R., 1992. Progressive deformation in anisotropic rocks. Journal of Structural Geology 14, 723–742.
Whitten, E.H.T., 1966. Structural Geology of Folded Rocks. Rand McNally & Company, Chicago.
Wood, D.S., 1974. Current views of the development of slaty cleavage. Annual Review of Earth and Planetary Sciences 2, 369–401.